

1. Introduction

High-throughput protein design and synthetic biology [6–8, 23, 25, 35, 55] increasingly depend on *in silico* estimates of the efficiency with which an enzyme converts a given substrate under realistic biochemical conditions. Turning this promise into practice requires accurate prediction of canonical kinetic constants [28, 39, 61], *e.g.*, k_{cat} , K_{m} , and K_{i} , directly from molecular inputs, so that large candidate libraries can be screened before any wet-lab investment. Yet current machine learning pipelines [5, 43, 50, 53] still struggle to move beyond dataset-specific correlations toward mechanism-aware generalization.

A central difficulty lies in how catalysis actually unfolds [6, 7, 25, 31, 35, 56], as “*Mutant Enzyme Reaction Mechanism*” in Figure 1. Early studies regressed kinetic constants from sequence alone [3, 36]. Subsequent multimodal systems encoded both the enzyme and the small-molecule substrate, typically via Protein Language Model (PLM) [17, 30, 37, 40] or CNN features for the sequence and SMILES/graph fingerprints for the substrate, and trained joint regressors [5, 28, 53, 61]. Examples include DLKcat [28] for k_{cat} from paired representations, UniKP [61] for multi-endpoint prediction with environmental covariates, and CataPro [53]/CatPred [5] that add stronger PLM features and uncertainty reporting. Despite progress, most pipelines [43, 53, 67] fuse the two branches with shallow operations (*e.g.*, concatenation and a single cross-attention layer) and then regress a score, implicitly treating catalysis as static compatibility. In reality, enzymes *first* recognize and position the substrate, *then* adapt pocket geometry [10, 27, 29, 33] to stabilize the transition state; both phases jointly determine k_{cat} , K_{m} , and K_{i} .

Transformer-based PLMs offer a principled prior for mechanism-aware modeling. Large-scale self-supervision yields embeddings that reflect evolutionary constraints, fold regularities, long-range contacts, and conserved catalytic motifs [2, 11, 12, 17, 30, 37, 44]. ESM families [17, 30, 37, 40] show that masked-token training captures structure-aware signals transferable to function tasks; ProtTrans/ProtT5 [11, 44] extend coverage with encoder-decoder modeling; Ankh/Ankh3 [2, 12] introduce protein-specific multi-task objectives that strengthen residue-level priors. These improved kinetic prediction when used as fixed inputs or lightly tuned backbones, and recent evidence supports careful fine-tuning [41]. Two gaps remain: PLMs are used passively rather than being explicitly conditioned on the concrete substrate, and naively injecting 3D evidence can dominate training and erode the biochemical semantics learned during pretraining [5, 43, 49, 53, 58, 68]. It motivates a formulation that conditions the PLM on substrate semantics and pocket geometry in a staged, mechanism-aligned manner while preserving its sequence-derived prior.

In light of this, we address these gaps by framing en-

zyme kinetics as *staged conditioning* aligned with enzymology: substrate recognition, then conformational adaptation (as shown in Figure 1). The proposed **Enzyme-Reaction Bridging Adapter (ERBA)** adapts to the PLM task in two phases. Stage 1, *Molecular Recognition Cross-Attention (MRCA)*, conditions the protein representation on the specific substrate to model selectivity and binding specificity. Stage 2, a *Geometry-aware Mixture-of-Experts (G-MoE)*, fuses the MRCA output with an active-site geometry encoder and routes each sample to pocket-specialized experts, capturing induced fit and conformational adaptation where catalysis occurs. To maintain adaptation stability, we introduce *Enzyme-Substrate Distribution Alignment (ESDA)*, which defines stability as distributional alignment in a reproducing kernel Hilbert space [65, 66] via an RBF-kernel maximum mean discrepancy. ESDA aligns the distributions of sequence-only, sequence-substrate, and sequence-substrate-structure representations to the PLM manifold, preserving biochemical semantics while allowing new substrate and geometry information to be expressed. Meanwhile, a heteroscedastic Gaussian [24] prediction head trained in \log_{10} space models the positivity of kinetic constants and their multiplicative noise.

In addition, we evaluate across three kinetic endpoints and multiple PLM backbones under consistent protocols. Extensive results demonstrate that shallow fusion underuses PLM priors and fails to capitalize on geometry, whereas ERBA’s staged conditioning yields consistent gains. Improvements hold across backbones of different scales, and cross-dataset tests indicate stronger out-of-distribution generalization, highlighting the benefit of conditioning the PLM first on substrate semantics and then on pocket geometry in a manner faithful to the catalytic mechanism.

In summary, our principal contributions are as follows:

- We propose a mechanism-aligned formulation of enzyme kinetics as staged conditioning from substrate recognition to pocket-level adaptation.
- We introduce an ERBA that combines MRCA for sequence-substrate fusion with a G-MoE that performs pocket-localized adaptation via sparse expert routing.
- We design an ESDA that aligns the sequence, substrate, and structure at the distribution level, preserving PLM biochemical semantics during multimodal fine-tuning.
- Evaluated across three kinetic endpoints and multiple PLM backbones, ERBA delivers consistent gains, offering a general interface for adding new modalities and improving out-of-distribution generalization.

2. Related Work

2.1. Enzyme Kinetic Parameter Prediction

Data-driven prediction of enzyme kinetics has progressed from sequence-only models to multimodal pipelines. Early

efforts such as DLKcat [28] coupled CNN/GNN encoders for protein sequences and substrate SMILES. Subsequent systems improved generalization by introducing PLM features [26, 43, 48, 53, 61]: TurNup [26] pairs ESM-1b [40] with reaction fingerprints in a boosted regressor; UniKP [61], MPEK [48], and CataPro [53] use ProtT5 [11] with SMILES to predict multiple endpoints; EITLEM [43] adopts ESM-1v [37] and residue-level attention for mutants. Despite these gains, most pipelines still operate on 1D sequence and 2D chemistry, leaving out the 3D pocket context that strongly influences k_{cat} , K_m , and K_i [29, 33, 50].

2.2. Transformer-based Protein Language Models

Transformer-based PLMs learn contextual protein representations from large sequence corpora [2, 11, 12, 17, 30, 37, 44, 47]. ESM models [30, 40] show that masked-token pretraining captures fold regularities, long-range contacts, and mutation sensitivity that transfer to structure and function tasks. ProtTrans/ProtT5 [11, 18] introduces encoder-decoder training and larger vocabularies, improving robustness for remote homologs. Ankh/Ankh3 [2, 12] adds protein-specific multitask objectives, strengthening residue-level priors. Scaling further enriches implicit structural knowledge, as in ESM-3 [17]. Such representations are now standard for kinetics because they encode evolutionary constraints, catalytic motifs, and physically plausible contacts.

2.3. Multimodal Integration for Enzyme Modeling

Catalysis reflects coupled effects of sequence, substrate chemistry, and conformational geometry. Recent integrations extend PLMs with structural or chemical modalities [20, 38, 51, 57, 68]. Examples include multimodal attention for active-site labeling [51], cross-modal regression with environmental factors [20], and combinations of cryo-EM or structure-derived features with PLM embeddings for molecular property prediction [9, 57, 62, 68]. Most works [5, 43, 48, 53], however, fuse modalities shallowly, which undercuts the mechanistic sequence of *recognition* then *adaptation* and risks destabilizing pretrained biochemical priors during fine-tuning. A staged, mechanism-aligned conditioning that injects substrate semantics first and pocket geometry second, while regularizing distributions to remain compatible with PLM space [4, 13], is thus warranted.

3. Methodology

3.1. Preliminaries

Problem Definition. The task of predicting enzyme kinetic parameters can be formulated as a conditional regression problem. Given an enzyme E with amino acid sequence $\mathbf{S}_e = \{s_i\}_{i=1, \dots, L_e}$, a substrate molecule \mathbf{S}_m (SMILES [19]) and their structural context \mathbf{S}_g , the goal is to predict quantitative kinetic parameters $\hat{\mathbf{y}} = \{k_{\text{cat}}, K_m, K_i\}$.

Formally, we aim to learn a multimodal regression function $f_\theta(\cdot)$ parameterized by θ :

$$\hat{\mathbf{y}} = f_\theta(\mathbf{S}_e, \mathbf{S}_m, \mathbf{S}_g), \quad \hat{\mathbf{y}} \in \mathbb{R}. \quad (1)$$

Existing Formulation. Most existing methods [5, 43, 48, 53] approximate f_θ by independently encoding the enzyme and substrate, followed by a shallow fusion and regression head to approximate:

$$\hat{\mathbf{y}} = \psi(\mathbf{S}_e \oplus \mathbf{S}_m \oplus \mathbf{S}_g), \quad (2)$$

where \oplus denotes concatenation and $\psi(\cdot)$ maps the fused representation to kinetic outputs. While straightforward, this performs only coarse feature aggregation and lacks fine-grained semantic alignment between molecular modalities. It implicitly treats catalysis as a static compatibility problem, ignoring the dynamic and hierarchical nature of enzymatic turnover-comprising (i) *substrate recognition* and (ii) *conformational adaptation* within the active site.

Mechanism-Aligned Formulation. We instead model enzymatic catalysis as a **staged conditional process**, in which kinetic behavior emerges from successive molecular interactions. Given that substrate binding determines selectivity and structural adaptation governs efficiency, we reformulate the prediction function as

$$\hat{\mathbf{y}} = f_\theta(\mathbf{S}_e | \mathbf{S}_m, \mathbf{S}_g) = f_\theta^{(2)}(f_\theta^{(1)}(\mathbf{S}_e, \mathbf{S}_m), \mathbf{S}_g). \quad (3)$$

Here, $f_\theta^{(1)}$ captures substrate-conditioned molecular recognition, and $f_\theta^{(2)}$ refines the representation through geometry-aware conformational adaptation. To realize this staged conditioning, we introduce the **Enzyme-Reaction Bridging Adapter (ERBA)** $\mathcal{A}(\cdot)$, which augments pretrained PLMs through hierarchical multimodal fusion. ERBA integrates two key modules: (i) the **Molecular Recognition Cross-Attention (MRCA)** $\mathcal{M}(\cdot)$ that injects substrate semantics into enzyme representations to model recognition specificity, and (ii) the **Geometry-aware Mixture-of-Experts (G-MoE)** $\mathcal{G}(\cdot)$ that incorporates three-dimensional structural cues to capture adaptive catalytic configurations. Formally, the PLM-based ERBA reformulates the staged conditioning in Eq. 3 as:

$$\hat{\mathbf{y}} = \mathcal{A}(\mathbf{S}_e | \mathbf{S}_m, \mathbf{S}_g) = \mathcal{G}^{(2)}\left(\underbrace{\mathcal{M}^{(1)}(\mathbf{S}_e, \mathbf{S}_m)}_{\text{(i) Substrate Recognition}}, \mathbf{S}_g\right), \quad (4)$$

(ii) Conformational Adaptation

where $\mathcal{M}^{(1)}$ performs substrate-conditioned fusion within the PLM latent space to align enzyme and substrate semantics, while $\mathcal{G}^{(2)}$ leverages local structural geometry to guide conformation-aware refinement. This hierarchical fusion mechanism enables biologically grounded and semantically aligned prediction of enzyme kinetic parameters, while preserving the biochemical priors inherent in pretrained PLMs.

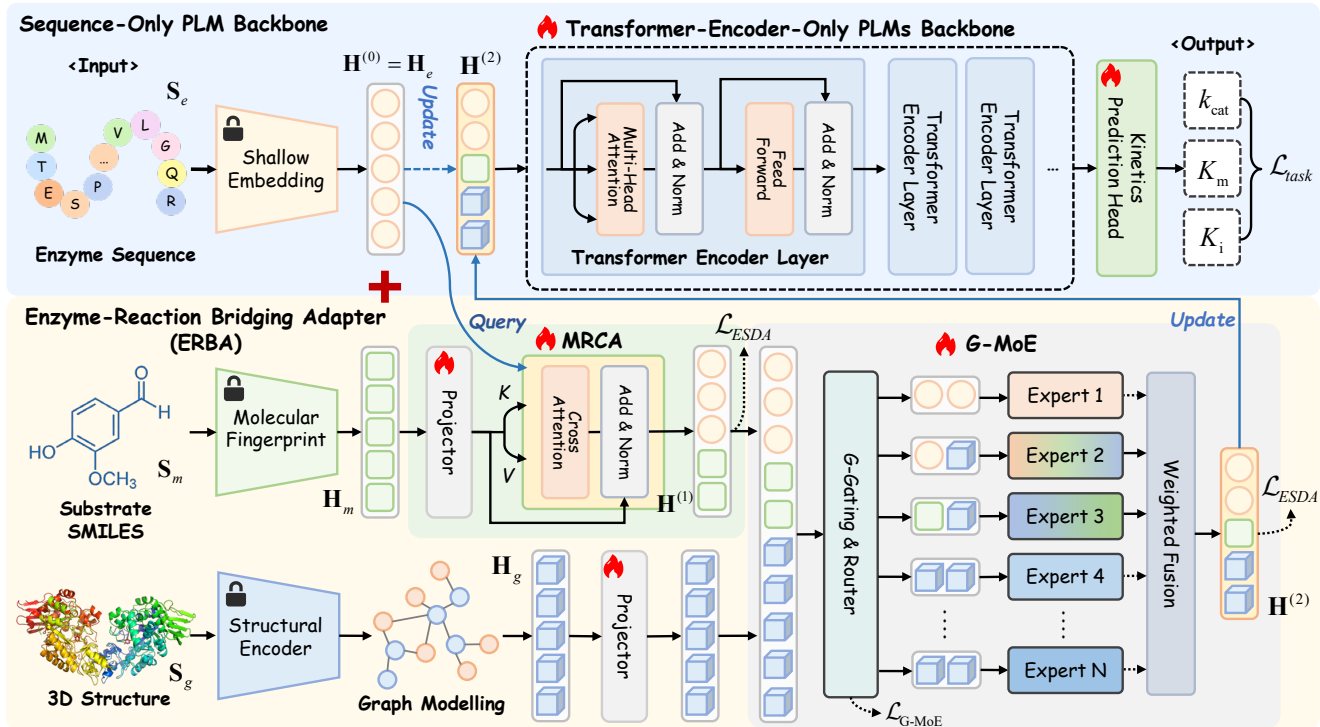


Figure 2. **Architecture of the proposed ERBA.** It augments a sequence-only PLM with multimodal conditioning on substrate chemistry and pocket geometry. MRCA injects substrate fingerprints into enzyme embeddings to capture recognition specificity, and G-MoE integrates local 3D pocket structure to model conformational adaptation. Update and query paths couple both modules to the backbone, while ESDA aligns representations with the prior PLM, enabling accurate prediction of enzyme kinetic parameters.

3.2. Molecular Recognition Cross-Attention

Catalysis begins with molecular recognition: substrate identity constrains selectivity and sets the context for subsequent conformational change. Let the enzyme sequence be $S_e \in \mathbb{R}^{L_e}$ and the substrate string be $S_m \in \mathbb{R}^{L_m}$. Shallow Transformer layers of the pretrained PLM act as an encoder that maps S_e to residue embeddings $H_e \in \mathbb{R}^{L_e \times D}$, preserving local biochemical cues while remaining amenable to multimodal conditioning. And the substrate tokens are embedded by MPNN encoder [60] guided by SMILES fingerprint priors [5], yielding $H_m \in \mathbb{R}^{L_m \times D}$. Recognition is cast as the proposed *Molecular Recognition Cross-Attention* (MRCA) module, which injects substrate semantics into the enzyme environment based on a single-layer cross-attention mechanism. With trainable projections $W_Q, W_K, W_V \in \mathbb{R}^{D \times d_k}$, we compute

$$\begin{aligned} A_{em} &= \text{Softmax}\left(\frac{(H_e W_Q)(H_m W_K)^T}{\sqrt{d_k}}\right), \\ Z_{em} &= A_{em}(H_m W_V), \end{aligned} \quad (5)$$

where $A_{em} \in \mathbb{R}^{L_e \times L_m}$ aligns enzyme tokens to substrate tokens and aggregates substrate-conditioned evidence. The resulting update $Z_{em} \in \mathbb{R}^{L_e \times D}$ is fused back to the enzyme stream with a residual connection and layer normalization, producing the substrate-aware representation

$H^{(1)} \in \mathbb{R}^{L_e \times D}$. This recognition-level summary highlights substrate-relevant residues and is passed to the next stage.

3.3. Geometry-aware Mixture-of-Experts

The second stage conditions recognition features on three-dimensional pocket geometry to model conformational adaptation at the catalytic site. Since pocket topology and residue packing induce heterogeneous geometric regimes that a shared adapter cannot capture [5], we introduce a *Geometry-aware Mixture-of-Experts* (G-MoE), whose routing depends jointly on recognition features and pocket structure in Figure 3. Let $H^{(1)} \in \mathbb{R}^{L_e \times D}$ denote the MRCA output and $\mathcal{P} \subset 1, \dots, L_e$ the pocket index set. Active-site tokens are encoded by an E-GNN [15] to yield geometry descriptors $H_g \in \mathbb{R}^{L_g \times D}$. We construct a joint routing vector v_{emg} via the G-Gating & Router module as:

$$v_{emg} = \left[\text{Pool}(H^{(1)}[\mathcal{P}]) \oplus \text{Pool}(H_g) \right] \in \mathbb{R}^{2D}, \quad (6)$$

where $\text{Pool}(\cdot)$ is tokenwise mean and $[\mathcal{P}]$ selects the pocket rows. Routing logits α and sparse gates $\tilde{\alpha}$ are then

$$\begin{aligned} \alpha &= \text{softmax}(W_{\text{gate}} v_{emg} + b_{\text{gate}}) \in \mathbb{R}^n, \\ \tilde{\alpha} &= \text{Top-}k(\alpha, k) \in \mathbb{R}^n, \end{aligned} \quad (7)$$

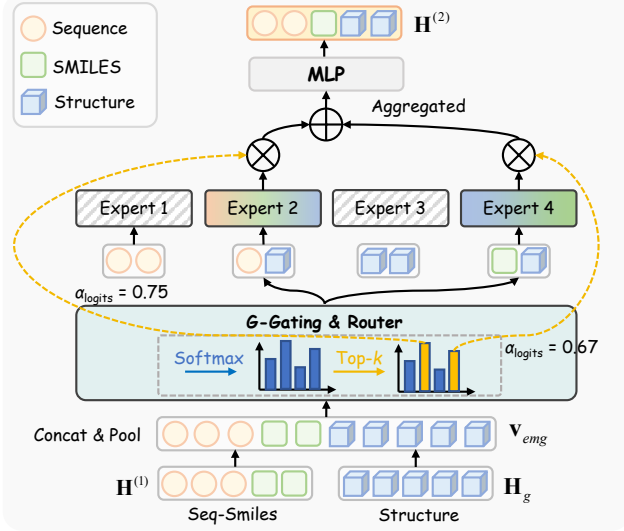


Figure 3. G-Gating & Router pools sequence-substrate and structural cues to produce gating logits, activate the top- k geometry-relevant experts, and suppress others. Selected experts transform structure-conditioned features, and an MLP fuses them into a geometry-adaptive representation for kinetic regression.

where only the k geometry-relevant experts are activated. In the model composed of n experts, each expert E_n performs a *pocket-local, geometry-modulated low-rank adaptation* by a geometry summary $\Gamma(\mathbf{H}_g) = \text{Pool}(\mathbf{H}_g) \in \mathbb{R}^D$:

$$E_n(\mathbf{H}^{(1)}, \mathbf{H}_g) = \mathbf{H}^{(1)} + \mathbf{V}_n \sigma \left(\mathbf{U}_n \mathbf{H}^{(1)}[\mathcal{P}] + \mathbf{B}_n \Gamma(\mathbf{H}_g) \right), \quad (8)$$

with $\mathbf{U}_n \in \mathbb{R}^{r \times D}$, $\mathbf{V}_n \in \mathbb{R}^{D \times r}$, and $\mathbf{B}_n \in \mathbb{R}^{r \times D}$ are learnable weight matrices, GELU nonlinearity σ , and $r \ll D$ is the rank of the adapter. Geometry thus conditions channel excitation within the pocket while leaving non-pocket residues unchanged, thereby aligning the learned adaptation with the structural determinants of the transition state.

Selected experts are aggregated to obtain the geometry-conditioned state used for kinetic regression as:

$$\mathbf{H}^{(2)} = \text{MLP} \left(\sum_{n \in \text{Top } k} \tilde{\alpha}_n E_n(\mathbf{H}^{(1)}, \mathbf{H}_g) \right) \in \mathbb{R}^D. \quad (9)$$

To prevent expert collapse while keeping geometry-driven sparsity, we add a light balancing term $\mathcal{L}_{\text{G-MoE}}$ that nudges the average gate mass toward uniform importance and the usage rate toward the expected Top- k proportion:

$$\mathcal{L}_{\text{G-MoE}} = \left\| \bar{\alpha} - \frac{1}{n} \mathbf{1} \right\|_2^2 + \left\| \bar{\mathbf{n}} - \frac{k}{n} \mathbf{1} \right\|_2^2, \quad (10)$$

where $\bar{\alpha} \in \mathbb{R}^n$ is the per-expert average of $\tilde{\alpha}$ over the current mini-batch, $\bar{\mathbf{n}} \in \mathbb{R}^n$ is the per-expert average of the indicator $\mathbf{1}[\tilde{\alpha} > 0]$ over the current mini-batch, $\mathbf{1} \in \mathbb{R}^n$ denotes the all-ones vector, and $\|\cdot\|_2$ is the Euclidean norm.

This regularizer is lightweight and does not dilute geometry guidance. In combination, geometry-driven routing, pocket-local adaptation, and sparse aggregation yield $\mathbf{H}^{(2)}$ that preserves global PLM priors, incorporates structural evidence at the catalytic site, and improves predictive fidelity for enzyme kinetics.

3.4. Enzyme-Substrate Distribution Alignment

Staged conditioning should absorb substrate and geometry signals while remaining compatible with the biochemical prior encoded by the pretrained PLM. To keep both stages anchored to this prior, let $\mathbf{H}^{(0)} = \mathbf{H}_e$ is the sequence embedding, $\mathbf{H}^{(1)}$ the substrate-conditioned embedding from MRCA, and $\mathbf{H}^{(2)}$ the geometry-conditioned representation from G-MoE. We introduce the *Enzyme-Substrate Distribution Alignment* (ESDA), inspired by kernel-based two-sample tests and distribution alignment techniques in statistical learning and transfer adaptation [16, 34, 52]. ESDA formalizes stability as distributional alignment in a reproducing kernel Hilbert space [65, 66], ensuring that recognition and adaptation evolve within the semantic domain of the PLM, rather than drifting into a new manifold. For this alignment, each stage’s global representation is summarized by averaging the embeddings across residues:

$$\mathcal{Z}^{(t)} = \frac{1}{L_e} \sum_{i=1}^{L_e} \mathbf{H}^{(t)}[i], \quad t \in \{0, 1, 2\}. \quad (11)$$

For any indices $a, b \in t$, using an RBF kernel $\kappa(\mathcal{Z}^a, \mathcal{Z}^b) = \exp(-\|\mathcal{Z}^a - \mathcal{Z}^b\|_2^2 / (2\sigma^2))$ with bandwidth σ set by the median heuristic [22], we adopt a diagonal-free, normalized mini-batch Maximum Mean Discrepancy (MMD) estimator [59] for any two sets $\mathcal{Z}^a, \mathcal{Z}^b$ of sizes N_a, N_b :

$$\begin{aligned} \widehat{\text{MMD}}^2(\mathcal{Z}^a, \mathcal{Z}^b) &= \frac{1}{N_a^2} \sum_{\substack{p, q \\ p \neq q}} \kappa(\mathcal{Z}_p^a, \mathcal{Z}_q^a) + \frac{1}{N_b^2} \sum_{\substack{p, q \\ p \neq q}} \kappa(\mathcal{Z}_p^b, \mathcal{Z}_q^b) \\ &\quad - \frac{2}{N_a N_b} \sum_{p, q} \kappa(\mathcal{Z}_p^a, \mathcal{Z}_q^b). \end{aligned} \quad (12)$$

In summary, ESDA anchors both stages to the PLM manifold and encourages a smooth progression from recognition to adaptation:

$$\mathcal{L}_{\text{ESDA}} = \widehat{\text{MMD}}^2(\mathcal{Z}^{(1)}, \mathcal{Z}^{(0)}) + \widehat{\text{MMD}}^2(\mathcal{Z}^{(2)}, \mathcal{Z}^{(0)}). \quad (13)$$

By aligning distributions rather than individual features, ESDA suppresses feature flooding from high-capacity geometric channels and mitigates forgetting of PLM biochemical semantics, while retaining information introduced by substrate identity and pocket geometry.

Method	Venue	Modality			Kinetic Endpoint: k_{cat}				Kinetic Endpoint: K_m				Kinetic Endpoint: K_i			
		S_e	S_m	S_g	$R^2\uparrow$	PCC \uparrow	RMSE \downarrow	MAE \downarrow	$R^2\uparrow$	PCC \uparrow	RMSE \downarrow	MAE \downarrow	$R^2\uparrow$	PCC \uparrow	RMSE \downarrow	MAE \downarrow
<i>Exp I: Existing SOTA Models</i>																
DLKcat [28]	Nat.Catal 2022	✓	✓	-	0.01	0.37	1.78	1.30	-	-	-	-	-	-	-	-
TurNup [26]	Nat.C 2023	✓	✓	-	0.39	0.65	1.60	1.19	-	-	-	-	-	-	-	-
UniKP [61]	Nat.C 2023	✓	✓	-	0.13	0.42	1.56	1.14	0.36	0.63	1.02	0.78	-	-	-	-
MPEK [48]	Brief.Bio 2024	✓	✓	-	0.33	0.59	1.34	1.05	0.30	0.56	1.40	1.09	-	-	-	-
EITLEM [43]	Chem.Catal 2024	✓	✓	-	0.34	0.63	1.35	0.80	0.30	0.59	1.06	0.82	0.38	0.70	1.33	0.97
CataPro [53]	Nat.C 2025	✓	✓	-	0.41	0.66	1.33	0.80	0.41	0.63	1.01	0.75	-	-	-	-
CatPred [5]	Nat.C 2025	✓	✓	✓	0.40	0.67	1.30	0.79	0.49	0.65	0.93	0.71	0.45	0.60	1.35	1.09
Ours[‡]	-	✓	✓	✓	0.54	0.74	1.13	0.74	0.61	0.79	0.70	0.61	0.61	0.78	1.26	0.91
<i>Exp II: Fine-tuning PLM Backbones</i>																
Ankh3-1.8B [2]	Arxiv 2025	✓	-	-	0.41	0.65	1.28	0.92	0.40	0.64	0.97	0.74	0.41	0.64	1.54	1.22
w/ ERBA	-	✓	✓	✓	0.50	0.72	1.17	0.80	0.51	0.72	0.88	0.66	0.52	0.73	1.39	1.06
Ankh3-5.7B [2]	Arxiv 2025	✓	-	-	0.43	0.67	1.24	0.88	0.42	0.65	0.98	0.74	0.46	0.68	1.47	1.15
w/ ERBA	-	✓	✓	✓	0.52	0.74	1.12	0.77	0.53	0.73	0.88	0.65	0.57	0.76	1.32	1.00
ProtT5-3B [18]	TPAMI 2021	✓	-	-	0.39	0.65	1.30	0.91	0.39	0.63	0.98	0.74	0.43	0.66	1.50	1.14
w/ ERBA	-	✓	✓	✓	0.47	0.71	1.22	0.85	0.54	0.74	0.88	0.65	0.58	0.76	1.31	0.97
ESM2-8M [30]	Science 2023	✓	-	-	0.19	0.43	1.49	1.11	0.26	0.51	1.08	0.84	0.15	0.39	1.82	1.46
w/ ERBA	-	✓	✓	✓	0.27	0.52	1.41	1.05	0.35	0.60	1.04	0.80	0.31	0.56	1.64	1.30
ESM2-35M [30]	Science 2023	✓	-	-	0.26	0.52	1.42	1.04	0.30	0.55	1.07	0.84	0.17	0.42	1.51	1.12
w/ ERBA	-	✓	✓	✓	0.38	0.62	1.31	0.96	0.38	0.62	1.01	0.78	0.34	0.59	1.60	1.26
ESM2-150M [30]	Science 2023	✓	-	-	0.30	0.55	1.38	1.01	0.33	0.58	1.04	0.80	0.33	0.58	1.62	1.29
w/ ERBA	-	✓	✓	✓	0.38	0.62	1.31	0.95	0.54	0.73	0.88	0.65	0.53	0.73	1.36	1.02
ESM2-650M [30]	Science 2023	✓	-	-	0.35	0.59	1.33	0.98	0.39	0.63	0.97	0.75	0.36	0.60	1.58	1.27
w/ ERBA	-	✓	✓	✓	0.44	0.66	1.25	0.91	0.55	0.74	0.81	0.64	0.53	0.74	1.35	0.99
ESM2-3B [30]	Science 2023	✓	-	-	0.41	0.65	1.27	0.92	0.43	0.66	0.94	0.72	0.49	0.71	1.38	1.05
w/ ERBA (Ours)	-	✓	✓	✓	0.54	0.74	1.13	0.74	0.61	0.79	0.70	0.61	0.61	0.78	1.26	0.91

Table 1. Performance comparison of existing SOTA methods and fine-tuned PLM backbones on enzyme kinetic prediction tasks. Results are presented for three kinetic parameters: turnover number (k_{cat}), Michaelis constant (K_m), and inhibition constant (K_i). The performance metrics include $R^2\uparrow$, PCC \uparrow , RMSE \downarrow , and MAE \downarrow . ERBA consistently outperforms the baselines across all metrics. Notably, the best value in each column is highlighted in red, and the second best in blue. [‡] indicates that the backbone of the PLMs is fine-tuned.

3.5. Enzyme Reaction Optimization

Kinetic constants are positive and affected by multiplicative noise, so we follow [5] to regress in \log_{10} space using a heteroscedastic Gaussian negative log-likelihood (NLL) [14]. For a target $y > 0$, let $z = \log_{10} y$. The prediction head outputs a mean μ and a log-variance $s = \log \sigma^2$ for z , yielding the per-sample NLL:

$$\mathcal{L}_{\text{task}} = \frac{1}{2} e^{-s} (z - \mu)^2 + \frac{1}{2} s. \quad (14)$$

Therefore, the full objective \mathcal{L} aggregates the likelihood through hyperparameter (λ_1, λ_2) modulation of task regularization $\mathcal{L}_{\text{task}}$, geometry-aware specialization $\mathcal{L}_{G\text{-MoE}}$, and distributional alignment $\mathcal{L}_{\text{ESDA}}$:

$$\mathcal{L} = \mathcal{L}_{\text{task}} + \lambda_1 \mathcal{L}_{G\text{-MoE}} + \lambda_2 \mathcal{L}_{\text{ESDA}}. \quad (15)$$

4. Experiments

4.1. Experimental Setup

Datasets. Following prior works [5, 43], we evaluate on three standard kinetic parameter prediction tasks: k_{cat} , K_m , and K_i , using data from BRENDA [42] and SABIO-RK [54]. The datasets contain 23,197 records for k_{cat} , 41,174 for K_m , and 11,929 for K_i . Each entry includes

a UniProt-validated enzyme sequence, substrate SMILES string, experimentally measured kinetic value, and associated 3D structure annotation. Compared to datasets used in DLKcat [28] and UniKP [61], we extend sequence and EC coverage, standardize molecular representations, and reduce integration biases, enabling controlled multimodal evaluation. Notably, in Section 4.2, we use the k_{cat} and K_m test sets from [43] for out-of-distribution generalization testing, where 3D structures are generated by OpenFold [1] or ESMFold [30]. Details are given in the Appendix.

Evaluation Metrics. We evaluate using mean absolute error (MAE) [28, 45], root mean square error (RMSE) [46, 53], Pearson correlation coefficient (PCC) [5], and coefficient of determination (R^2) [5, 28, 43]. All metrics are computed on \log_{10} transformed targets for k_{cat} , K_m , and K_i to stabilize scale and variance. Lower MAE and RMSE and higher PCC and R^2 indicate better performance. Unless noted otherwise, results are averaged over repeated runs with fixed data splits and identical preprocessing.

Implementation Details. The enzyme-encoding process employs a PLM with a latent dimension of $D = 1024$ and a fixed tokenization scheme. Sequences are truncated or padded to a maximum length $L_e = 1024$. The substrate is encoded from a canonical SMILES and mapped to dimen-

Index	Class Name	Count	Kinetic Endpoint: k_{cat}				Count	Kinetic Endpoint: K_m				Count	Kinetic Endpoint: K_i			
			R ² ↑	PCC↑	RMSE↓	MAE↓		R ² ↑	PCC↑	RMSE↓	MAE↓		R ² ↑	PCC↑	RMSE↓	MAE↓
EC-1	<i>Oxidoreductases</i>	679	0.37	0.62	1.32	0.95	1,382	0.55	0.74	0.90	0.69	282	0.58	0.77	1.19	0.92
EC-2	<i>Transferases</i>	334	0.46	0.69	1.22	0.87	1,000	0.53	0.73	0.81	0.61	270	0.38	0.65	1.37	0.99
EC-3	<i>Hydrolases</i>	682	0.43	0.68	1.18	0.88	1,145	0.51	0.72	0.90	0.65	408	0.48	0.71	1.50	1.10
EC-4	<i>Lyases</i>	131	0.50	0.71	1.27	0.92	293	0.56	0.75	0.81	0.61	157	0.65	0.81	1.19	0.84
EC-5	<i>Isomerases</i>	72	0.46	0.73	1.39	0.94	123	0.61	0.78	0.84	0.64	42	0.67	0.83	1.20	0.95
EC-6	<i>Ligases</i>	48	0.53	0.77	0.96	0.71	135	0.34	0.59	1.02	0.76	21	0.34	0.62	1.39	1.03

Table 2. **Enzyme category analysis across kinetic prediction tasks.** The table provides a breakdown of enzyme categories in the datasets for k_{cat} , K_m , and K_i prediction tasks. It includes the distribution of each enzyme class, the number of samples per category, and performance metrics for each class. Notably, the best value in each column is highlighted in red, and the second best in blue.

Method	OOD Test @EITLEM- k_{cat}				OOD Test @EITLEM- K_m			
	R ² ↑	PCC↑	RMSE↓	MAE↓	R ² ↑	PCC↑	RMSE↓	MAE↓
DLKcat [28]	0.01	0.15	3.87	3.05	-	-	-	-
TurNup [26]	0.21	0.38	2.46	2.11	-	-	-	-
UniKP [61]	0.08	0.20	1.76	1.24	0.14	0.32	1.54	1.08
MPEK [48]	0.17	0.41	1.65	1.18	0.12	0.35	1.71	1.32
EITLEM [43]	0.27	0.50	1.43	0.95	0.23	0.43	1.31	1.03
CataPro [53]	0.25	0.47	1.59	1.08	0.27	0.41	1.23	0.96
CatPred [5]	0.25	0.46	1.50	1.03	0.30	0.45	1.11	0.87
Ours [‡]	0.50	0.70	1.21	0.81	0.55	0.69	0.79	0.69

Table 3. **Comparison with existing SOTA models on OOD tests.** k_{cat} and K_m using the EITLEM [43] test sets.

sion D via a linear layer; pocket geometry is computed from active-site residues, and its channels are projected to D via another linear layer. G-MoE employs $n = 4$ experts with top $k = 2$ routing. We evaluate ProtT5 [18], ESM2 [30], and Ankh3 [2] backbones to verify robustness across PLMs. For parameter-efficient adaptation, LoRA [21] is applied to the top PLM layers with a rank of 8, a scaling factor of 16, and a dropout rate of 0.1. Training uses AdamW [32] with learning rate 1×10^{-4} . In full objective \mathcal{L} , the hyperparameters are set to $\lambda_1 = 0.01$ and $\lambda_2 = 0.1$.

4.2. Performance Analysis

We benchmark ours (ESM2-3B w/ ERBA) against recent methods on k_{cat} , K_m , and K_i , reimplementing all baselines with the same ESM2-3B enzyme encoder for fairness.

Performance Comparison. As shown in Exp I of Table 1, our method outperforms existing SOTA models across all three kinetic parameters. For k_{cat} , we achieve an R^2 of 0.54, a notable improvement over CatPro’s 0.41, along with superior PCC (0.74 vs. 0.67) and lower RMSE (0.79 vs. 1.30). For K_m , our model leads with an R^2 of 0.61, compared to CatPro’s 0.49, and a lower RMSE of 0.70. Similarly, for K_i , we achieve a PCC of 0.78 and reduce RMSE to 1.26, outperforming CatPro’s 0.60 and 1.35, respectively. These results underscore the effectiveness of our approach, which combines sequence and substrate information via ERBA to enable accurate modeling of enzyme-substrate interactions.

Backbone Scaling and the Effect of ERBA. We next examine whether ERBA’s gains persist across PLM scales

and families in Exp II of Table 1. Across ESM2 (8M \rightarrow 3B), ProtT5-3B, and Ankh3 (1.8B/5.7B), attaching ERBA to the same backbone consistently improves all three endpoints. On ESM2-3B, k_{cat} rises from $R^2=0.41$ to 0.54 with higher PCC (0.74) and lower RMSE (0.79); K_m climbs from $R^2=0.43$ to 0.61 with RMSE dropping to 0.70; K_i sees PCC improve from 0.71 to 0.78 while RMSE falls from 1.38 to 1.26. Similar trends hold at smaller scales (8M /35M /150M /650M) and on non-ESM backbones (ProtT5-3B, Ankh3), indicating that ERBA provides orthogonal benefits to model size and pretraining recipe. Scaling the backbone alone yields moderate gains, but adding ERBA produces larger, more uniform improvements, especially on K_m and K_i where structural context matters most.

Performance Representation of Enzyme Distribution.

Table 2 presents the performance across six enzyme classes for the kinetic parameters k_{cat} , K_m , and K_i . Our model performs best for EC-4 (Lyases), achieving high R^2 and PCC values, particularly for K_i and k_{cat} . EC-6 (Ligases) shows lower performance, particularly in K_m and K_i . These results demonstrate the model’s overall robustness while highlighting challenges in predicting certain kinetic parameters for specific enzyme classes.

Error Distribution Analysis. Figure 4 shows the log-scaled experimental vs. predicted values for k_{cat} , K_m , and K_i , with 1-Radio_{AE} indicating the percentage of predictions with absolute errors ≤ 1 . The dashed red line represents perfect predictions. Overall, the model demonstrates good performance, with 1-Radio_{AE} values of 67.67% for k_{cat} , 62.28% for K_i , and 79.53% for K_m . K_m predictions are more concentrated around the perfect prediction line, while k_{cat} shows more variation. These results highlight the model’s robustness and suggest that further improvement is needed, particularly for k_{cat} and K_i .

Out-of-Distribution Generalization. To evaluate OOD generalization, we compare our method with SOTA models on k_{cat} and K_m using the EITLEM test sets [43]. Our model consistently outperforms all other methods. For k_{cat} , we achieve the highest R^2 (0.50) and PCC (0.70), outperforming EITLEM ($R^2 = 0.27$, PCC = 0.50) and others. For K_m , we achieve R^2 of 0.55 and PCC of 0.69, surpassing

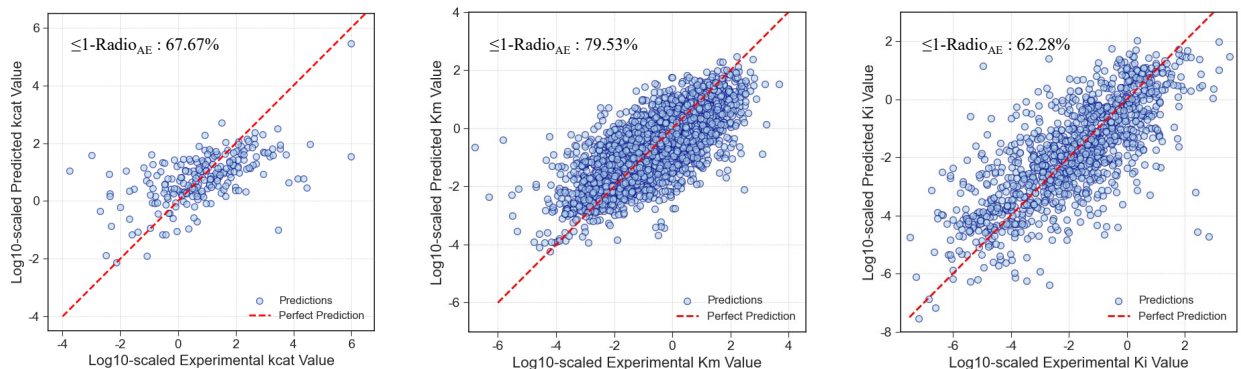


Figure 4. **Log-scaled experimental versus predicted values for the kinetic parameters k_{cat} , K_m , and K_i .** Each plot shows the absolute error less than or equal to 1 as a percentage, denoted as $1-Radio_{AE}$. The dashed red line represents perfect predictions.

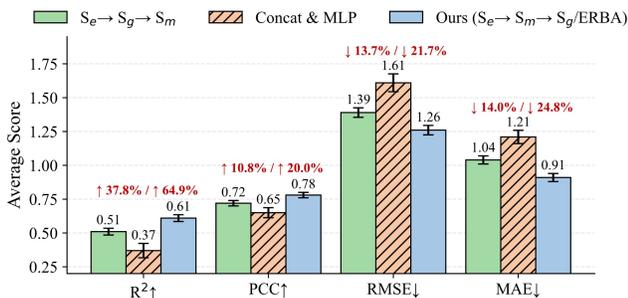


Figure 5. **Ablation studies on fusion order and manner.** Comparison of different fusion strategies: $S_e \rightarrow S_g \rightarrow S_m$, Concat & MLP, and the proposed $S_e \rightarrow S_m \rightarrow S_g/ERBA$. Percentage improvements across metrics are highlighted in red.

SOTA models by a clear margin. These results show that leveraging PLMs as dynamic backbones, rather than fixed priors, enables superior generalization. Our ERBA adapts the PLM’s pre-trained knowledge to specific substrate and structural contexts, providing enhanced flexibility. This approach improves the model’s ability to generalize across unseen enzyme-substrate pairs, giving it a clear advantage over models that use PLMs passively.

4.3. Ablation Study

Do the Modules Add Gains? We assess the contribution of each module by progressively adding MRCA, G-MoE, and ESDA to the PLM baseline. In Table 4, MRCA improves R^2 from 0.49 to 0.51 and PCC from 0.71 to 0.73, enhancing substrate recognition. Adding G-MoE further refines the model, increasing R^2 to 0.54 and PCC to 0.74. Finally, the complete ESDA framework achieves the best performance with R^2 of 0.61 and PCC of 0.78, demonstrating the value of distribution alignment for preserving PLM semantics while incorporating substrate and geometry.

Does Fusion Order Matter? The results show that the fusion order significantly impacts model performance. Specifically, the $S_e \rightarrow S_m \rightarrow S_g/ERBA$ fusion consistently

Method	Modality			Kinetic Endpoint: K_i			
	S_e	S_m	S_g	$R^2 \uparrow$	PCC \uparrow	RMSE \downarrow	MAE \downarrow
PLM Baseline	✓	-	-	0.49	0.71	1.38	1.05
w/ MRCA	✓	✓	-	0.51	0.73	1.32	0.98
w/ G-MoE	✓	✓	✓	0.54	0.74	1.27	0.94
w/ ESDA (Ours)	✓	✓	✓	0.61	0.78	1.26	0.91

Table 4. **Ablation study on the effect of different modules.** Performance comparison for K_i prediction with various configurations: PLM baseline, MRCA, G-MoE, and our ESDA framework.

outperforms the $S_e \rightarrow S_g \rightarrow S_m$ configuration across all metrics. This demonstrates that first aligning the enzyme sequence with substrate information before incorporating structural context leads to better model generalization. The observed improvement in R^2 (37.8%) and a reduction in RMSE (20%) highlight the importance of this fusion order for accurate enzyme kinetic predictions.

Is ESBA Better than Concatenation? The comparison between our ESBA and simple concatenation with MLP [63, 64] highlights the advantage of incorporating distributional alignment. ESBA improves model performance, yielding a 20% increase in PCC and a 14% reduction in MAE compared to concatenation. It demonstrates ESBA by aligning the representations at the distribution level, preserving the pretrained biochemical priors while effectively integrating the substrate and structural information.

5. Conclusion

We frame enzyme kinetics as mechanism-aligned staged conditioning, not static compatibility, and propose ERBA, which fine-tunes PLMs with MRCA for substrate-conditioned representations and G-MoE for pocket-aware fusion with geometry. ESDA enforces distributional alignment among sequence, sequence-substrate, and sequence-substrate-structure so that new modalities refine rather than overwrite its prior, yielding consistent gains and stronger out-of-distribution generalization, and offering a compact recipe for future multimodal PLMs that tightly couple sequence, molecular graphs, and geometry.

6. Acknowledgments

This research was supported by the Natural Science Foundation of Anhui Province (2408085MC051, 2408085MF159), the Key Science & Technology Project of Anhui Province (202304a05020068, 202423110050064), the National Natural Science Foundation of China (U24A20331), and the Fundamental Research Funds for the Central Universities of China (PA2025IISL0109, JZ2023HGQA0472). Yanyan Wei is the corresponding author.

References

- [1] Gustaf Ahdritz, Nazim Bouatta, Christina Floristean, Sachin Kadyan, Qinghui Xia, William Gerecke, Timothy J O'Donnell, Daniel Berenberg, Ian Fisk, Niccolò Zanichelli, et al. Openfold: Retraining alphafold2 yields new insights into its learning mechanisms and capacity for generalization. *Nature methods*, 21(8):1514–1524, 2024. [6](#), [14](#)
- [2] Hazem Alsamkary, Mohamed Elshaffei, Mohamed Elkerdawy, and Ahmed Elnaggar. Ankh3: Multi-task pretraining with sequence denoising and completion enhances protein representations. *arXiv preprint arXiv:2505.20052*, 2025. [2](#), [3](#), [6](#), [7](#), [14](#), [15](#), [16](#)
- [3] Shiran Barber-Zucker, Vladimir Mindel, Eva Garcia-Ruiz, Jonathan J Weinstein, Miguel Alcalde, and Sarel J Fleishman. Stable and functionally diverse versatile peroxidases designed directly from sequences. *Journal of the American Chemical Society*, 144(8):3564–3571, 2022. [2](#)
- [4] Manojit Bhattacharya, Soumen Pal, Srijan Chatterjee, Sang-Soo Lee, and Chiranjib Chakraborty. Large language model to multimodal large language model: A journey to shape the biological macromolecules to biological sciences and medicine. *Molecular Therapy Nucleic Acids*, 35(3), 2024. [3](#)
- [5] Veda Sheers Boorla and Costas D Maranas. Catpred: a comprehensive framework for deep learning in vitro enzyme kinetic parameters. *Nature communications*, 16(1):2072, 2025. [2](#), [3](#), [4](#), [6](#), [7](#), [12](#), [13](#)
- [6] R Buller, S Lutz, RJ Kazlauskas, R Snajdrova, JC Moore, and UT Bornscheuer. From nature to industry: Harnessing enzymes for biocatalysis. *Science*, 382(6673):eadh8615, 2023. [2](#)
- [7] Yanchun Chen, Jinyuan Sun, Kelun Shi, Tong Zhu, Ruifeng Li, Ruiqiao Li, Xiaomeng Liu, Xinying Xie, Chao Ding, Wen-Chao Geng, et al. Glycolysis-compatible urethanases for polyurethane recycling. *Science*, 390(6772):503–509, 2025. [2](#)
- [8] Gregory B Craven, Dominic P Affron, Charlotte E Allen, Stefan Matthies, Joe G Greener, Rhodri ML Morgan, Edward W Tate, Alan Armstrong, and David J Mann. High-throughput kinetic analysis for target-directed covalent ligand discovery. *Angewandte Chemie International Edition*, 57(19):5257–5261, 2018. [2](#)
- [9] Yifan Deng, Spencer S Ericksen, and Anthony Gitter. Chemical language model linker: blending text and molecules with modular adapters. *Journal of Chemical Information and Modeling*, 65(17):8944–8956, 2025. [3](#)
- [10] Mengze Du, Fei Wang, Yu Wang, Kun Li, Wenhui Hou, Lu Liu, Yong He, and Yuwei Wang. Improving long-tailed pest classification using diffusion model-based data augmentation. *Computers and Electronics in Agriculture*, 234:110244, 2025. [2](#)
- [11] Ahmed Elnaggar, Michael Heinzinger, Christian Dallago, Ghalia Rehawi, Yu Wang, Llion Jones, Tom Gibbs, Tamas Feher, Christoph Angerer, Martin Steinegger, et al. Prottrans: Toward understanding the language of life through self-supervised learning. *IEEE transactions on pattern analysis and machine intelligence*, 44(10):7112–7127, 2021. [2](#), [3](#), [15](#), [16](#)
- [12] Ahmed Elnaggar, Hazem Essam, Wafaa Salah-Eldin, Walid Moustafa, Mohamed Elkerdawy, Charlotte Rochereau, and Burkhard Rost. Ankh: Optimized protein language model unlocks general-purpose modelling. *arXiv preprint arXiv:2301.06568*, 2023. [2](#), [3](#)
- [13] Sam Gelman, Bryce Johnson, Chase R Freschlin, Arnav Sharma, Sameer D'Costa, John Peters, Anthony Gitter, and Philip A Romero. Biophysics-based protein language models for protein engineering. *Nature Methods*, pages 1–12, 2025. [3](#)
- [14] Pascal Germain, Francis Bach, Alexandre Lacoste, and Simon Lacoste-Julien. Pac-bayesian theory meets bayesian inference. *Advances in Neural Information Processing Systems*, 29, 2016. [6](#)
- [15] Joe G Greener and Kiarash Jamali. Fast protein structure searching using structure graph embeddings. *Bioinformatics Advances*, 5(1):vbaf042, 2025. [4](#)
- [16] Lan-Zhe Guo, Zhi Zhou, Yu-Feng Li, and Zhi-Hua Zhou. Identifying useful learnwares for heterogeneous label spaces. In *International Conference on Machine Learning*, pages 12122–12131, 2023. [5](#)
- [17] Thomas Hayes, Roshan Rao, Halil Akin, Nicholas J Sofroniew, Deniz Oktay, Zeming Lin, Robert Verkuil, Vincent Q Tran, Jonathan Deaton, Marius Wiggert, et al. Simulating 500 million years of evolution with a language model. *Science*, 387(6736):850–858, 2025. [2](#), [3](#)
- [18] Michael Heinzinger, Konstantin Weissenow, Joaquin Gomez Sanchez, Adrian Henkel, Milot Mirdita, Martin Steinegger, and Burkhard Rost. Bilingual language model for protein sequence and structure. *NAR Genomics and Bioinformatics*, 6(4):lqae150, 2024. [3](#), [6](#), [7](#), [14](#)
- [19] Shion Honda, Shoi Shi, and Hiroki R Ueda. Smiles transformer: Pre-trained molecular fingerprint for low data drug discovery. *arXiv preprint arXiv:1911.04738*, 2019. [3](#)
- [20] Bozhen Hu, Cheng Tan, Siyuan Li, Jiangbin Zheng, Sizhe Qiu, Jun Xia, and Stan Z Li. Multimodal regression for enzyme turnover rates prediction. *arXiv preprint arXiv:2509.11782*, 2025. [3](#)
- [21] Edward J Hu, Yelong Shen, Phillip Wallis, Zeyuan Allen-Zhu, Yuanzhi Li, Shean Wang, Lu Wang, Weizhu Chen, et al. Lora: Low-rank adaptation of large language models. *ICLR*, 1(2):3, 2022. [7](#)
- [22] Sadeep Jayasumana, Richard Hartley, Mathieu Salzmann, Hongdong Li, and Mehrtaash Harandi. Kernel methods on

- riemannian manifolds with gaussian rbf kernels. *IEEE transactions on pattern analysis and machine intelligence*, 37(12): 2464–2477, 2015. 5
- [23] ET Kaiser and DS Lawrence. Chemical mutation of enzyme active sites. *Science*, 226(4674):505–511, 1984. 2
- [24] Kristian Kersting, Christian Plagemann, Patrick Pfaff, and Wolfram Burgard. Most likely heteroscedastic gaussian process regression. In *Proceedings of the 24th international conference on Machine learning*, pages 393–400, 2007. 2
- [25] Daniel A Kraut, Kate S Carroll, and Daniel Herschlag. Challenges in enzyme mechanism and energetics. *Annual review of biochemistry*, 72(1):517–571, 2003. 2
- [26] Alexander Kroll, Yvan Rousset, Xiao-Pan Hu, Nina A Liebrand, and Martin J Lercher. Turnover number predictions for kinetically uncharacterized enzymes using machine and deep learning. *Nature communications*, 14(1):4139, 2023. 3, 6, 7, 12
- [27] Nelson J Leonard. Dimensional probes of enzyme-coenzyme binding sites. *Accounts of Chemical Research*, 15(5):128–135, 1982. 2
- [28] Feiran Li, Le Yuan, Hongzhong Lu, Gang Li, Yu Chen, Martin KM Engqvist, Eduard J Kerkhoven, and Jens Nielsen. Deep learning-based k_{cat} prediction enables improved enzyme-constrained model reconstruction. *Nature Catalysis*, 5(8):662–672, 2022. 2, 3, 6, 7, 12
- [29] Yang Li, Yixin Wang, Xueying Zheng, Jinjiang Guo, and Rumin Zhang. Dcbk: A fragment-based hybrid simulation and machine learning framework for predicting ligand dissociation kinetics. *bioRxiv*, pages 2025–11, 2025. 2, 3
- [30] Zeming Lin, Halil Akin, Roshan Rao, Brian Hie, Zhongkai Zhu, Wenting Lu, Nikita Smetanin, Robert Verkuil, Ori Kabeli, Yaniv Shmueli, et al. Evolutionary-scale prediction of atomic-level protein structure with a language model. *Science*, 379(6637):1123–1130, 2023. 2, 3, 6, 7, 12, 14, 15, 16
- [31] Tiantao Liu, Silong Zhai, Xinke Zhan, and Shirley WI Siu. Data-driven revolution of enzyme catalysis from the perspective of reactions, pathways, and enzymes. *Cell Reports Physical Science*, 6(3), 2025. 2
- [32] Ilya Loshchilov and Frank Hutter. Decoupled weight decay regularization. *arXiv preprint arXiv:1711.05101*, 2017. 7
- [33] Ding Luo, Xiaoyang Qu, and Binju Wang. Catalytic pocket-informed augmentation of enzyme kinetic parameters prediction via hierarchical graph learning. *bioRxiv*, pages 2025–05, 2025. 2, 3
- [34] Shaogao Lv and Heng Lian. Debiased distributed learning for sparse partial linear models in high dimensions. *Journal of Machine Learning Research*, 23(2):1–32, 2022. 5
- [35] Craig James Markin, Daniel Alexander Mokhtari, F Sunden, MJ Appel, E Akiva, SA Longwell, C Sabatti, D Herschlag, and PM Fordyce. Revealing enzyme functional architecture via high-throughput microfluidic enzyme kinetics. *Science*, 373(6553):eabf8761, 2021. 2
- [36] Stanislav Mazurenko, Zbynek Prokop, and Jiri Damborsky. Machine learning in enzyme engineering. *ACS catalysis*, 10(2):1210–1223, 2019. 2
- [37] Joshua Meier, Roshan Rao, Robert Verkuil, Jason Liu, Tom Sercu, and Alex Rives. Language models enable zero-shot prediction of the effects of mutations on protein function. *Advances in neural information processing systems*, 34:29287–29303, 2021. 2, 3
- [38] Song Ouyang, Huiyu Cai, Yong Luo, Kehua Su, Lefei Zhang, and Bo Du. Mmsite: A multi-modal framework for the identification of active sites in proteins. *Advances in Neural Information Processing Systems*, 37:45819–45849, 2024. 3
- [39] Ruijie Quan, Wenguan Wang, Fan Ma, Hehe Fan, and Yi Yang. Clustering for protein representation learning. In *Proceedings of the IEEE/CVF conference on computer vision and pattern recognition*, pages 319–329, 2024. 2
- [40] Alexander Rives, Joshua Meier, Tom Sercu, Siddharth Goyal, Zeming Lin, Jason Liu, Demi Guo, Myle Ott, C Lawrence Zitnick, Jerry Ma, et al. Biological structure and function emerge from scaling unsupervised learning to 250 million protein sequences. *Proceedings of the National Academy of Sciences*, 118(15):e2016239118, 2021. 2, 3
- [41] Robert Schmirler, Michael Heinzinger, and Burkhard Rost. Fine-tuning protein language models boosts predictions across diverse tasks. *Nature Communications*, 15(1):7407, 2024. 2
- [42] Ida Schomburg, Antje Chang, Christian Ebeling, Marion Gremse, Christian Heldt, Gregor Huhn, and Dietmar Schomburg. Brenda, the enzyme database: updates and major new developments. *Nucleic acids research*, 32(suppl_1):D431–D433, 2004. 6, 12
- [43] Xiaowei Shen, Ziheng Cui, Jianyu Long, Shiding Zhang, Biqiang Chen, and Tianwei Tan. Eitlem-kinetics: A deep-learning framework for kinetic parameter prediction of mutant enzymes. *Chem Catalysis*, 4(9), 2024. 2, 3, 6, 7, 12, 13, 14
- [44] Timothy Truong Jr and Tristan Bepler. Poet: A generative model of protein families as sequences-of-sequences. *Advances in Neural Information Processing Systems*, 36: 77379–77415, 2023. 2, 3
- [45] Fei Wang, Dan Guo, Kun Li, and Meng Wang. Eulermormer: Robust eulerian motion magnification via dynamic filtering within transformer. In *Proceedings of the AAAI Conference on Artificial Intelligence*, pages 5345–5353, 2024. 6
- [46] Fei Wang, Dan Guo, Kun Li, Zhun Zhong, and Meng Wang. Frequency decoupling for motion magnification via multi-level isomorphic architecture. In *Proceedings of the IEEE/CVF Conference on Computer Vision and Pattern Recognition*, pages 18984–18994, 2024. 6
- [47] Fei Wang, Kun Li, Yiqi Nie, Zhangling Duan, Peng Zou, Zhiliang Wu, Yuwei Wang, and Yanyan Wei. Exploiting ensemble learning for cross-view isolated sign language recognition. In *Companion Proceedings of the ACM on Web Conference 2025*, pages 2453–2457, 2025. 3
- [48] Jingjing Wang, Zhijiang Yang, Chang Chen, Ge Yao, Xiukun Wan, Shaoheng Bao, Junjie Ding, Liangliang Wang, and Hui Jiang. Mpek: a multitask deep learning framework based on pretrained language models for enzymatic reaction kinetic parameters prediction. *Briefings in Bioinformatics*, 25(5): bbae387, 2024. 3, 6, 7

- [49] Mengyu Wang, Zhenyu Liu, Kun Li, Yu Wang, Yuwei Wang, Yanyan Wei, and Fei Wang. Task-generalized adaptive cross-domain learning for multimodal image fusion. *IEEE Transactions on Multimedia*, 2026. 2
- [50] Weijia Wang, Fei Wang, Zhongzhen Wang, Xianyang Shi, and Chunyan Xu. Robust s3former deep learning model for the direct diagnosis and prediction of natural organic matter (nom) from three-dimensional excitation-emission-matrix (3d-eem) data. *Water Research*, 284:123994, 2025. 2, 3
- [51] Xiaorui Wang, Xiaodan Yin, Dejun Jiang, Hui Feng Zhao, Zhenxing Wu, Odin Zhang, Jike Wang, Yuquan Li, Yafeng Deng, Huanxiang Liu, et al. Multi-modal deep learning enables efficient and accurate annotation of enzymatic active sites. *Nature Communications*, 15(1):7348, 2024. 3
- [52] Yuhao Wang, Junwei Pan, Pengyue Jia, Wanyu Wang, Maolin Wang, Zhixiang Feng, Xiaotian Li, Jie Jiang, and Xiangyu Zhao. Pre-train, align, and disentangle: Empowering sequential recommendation with large language models. In *Proceedings of the 48th International ACM SIGIR Conference on Research and Development in Information Retrieval*, pages 1455–1465, 2025. 5
- [53] Zechen Wang, Dongqi Xie, Dong Wu, Xiaozhou Luo, Sheng Wang, Yangyang Li, Yanmei Yang, Weifeng Li, and Liangzhen Zheng. Robust enzyme discovery and engineering with deep learning using catapro. *Nature communications*, 16(1):2736, 2025. 2, 3, 6, 7
- [54] Ulrike Wittig, Renate Kania, Martin Golebiewski, Maja Rey, Lei Shi, Lenneke Jong, Enkhjargal Alгаа, Andreas Weidemann, Heidrun Sauer-Danzwith, Saqib Mir, et al. Sabiorck—database for biochemical reaction kinetics. *Nucleic acids research*, 40(D1):D790–D796, 2012. 6, 12
- [55] Richard Wolfenden and Mark J Snider. The depth of chemical time and the power of enzymes as catalysts. *Accounts of chemical research*, 34(12):938–945, 2001. 2
- [56] Tao Wu, Yinmiao Wang, Ningxin Zhang, Dejing Yin, Yan Xu, Yao Nie, and Xiaoqing Mu. Reshaping substrate-binding pocket of leucine dehydrogenase for bidirectionally accessing structurally diverse substrates. *ACS Catalysis*, 13(1): 158–168, 2022. 2
- [57] Hongwang Xiao, Wenjun Lin, Xi Chen, Hui Wang, Kai Chen, Jiashan Li, Yuancheng Sun, Sicheng Dai, Boya Wu, and Qiwei Ye. Stella: Towards protein function prediction with multimodal llms integrating sequence-structure representations. *arXiv preprint arXiv:2506.03800*, 2025. 3
- [58] Yang Xue, Zijing Liu, Xiaomin Fang, and Fan Wang. Multimodal pre-training model for sequence-based prediction of protein-protein interaction. In *Machine Learning in Computational Biology*, pages 34–46, 2022. 2
- [59] Hongliang Yan, Yukang Ding, Peihua Li, Qilong Wang, Yong Xu, and Wangmeng Zuo. Mind the class weight bias: Weighted maximum mean discrepancy for unsupervised domain adaptation. In *Proceedings of the IEEE conference on computer vision and pattern recognition*, pages 2272–2281, 2017. 5
- [60] Kevin Yang, Kyle Swanson, Wengong Jin, Connor Coley, Philipp Eiden, Hua Gao, Angel Guzman-Perez, Timothy Hopper, Brian Kelley, Miriam Mathea, et al. Analyzing learned molecular representations for property prediction. *Journal of chemical information and modeling*, 59(8):3370–3388, 2019. 4
- [61] Han Yu, Huaxiang Deng, Jiahui He, Jay D Keasling, and Xiaozhou Luo. Unikp: a unified framework for the prediction of enzyme kinetic parameters. *Nature communications*, 14(1):8211, 2023. 2, 3, 6, 7
- [62] Qianmu Yuan, Chong Tian, Yidong Song, Peihua Ou, Mingming Zhu, Huiying Zhao, and Yuedong Yang. Gpsfun: geometry-aware protein sequence function predictions with language models. *Nucleic Acids Research*, 52(W1):W248–W255, 2024. 3
- [63] Renrui Zhang, Jiaming Han, Chris Liu, Aojun Zhou, Pan Lu, Yu Qiao, Hongsheng Li, and Peng Gao. Llama-adapter: Efficient fine-tuning of large language models with zero-initialized attention. In *The Twelfth International Conference on Learning Representations*, 2024. 8
- [64] Tianren Zhang and Dai-Bei Yang. Multimodal machine learning with large language embedding model for polymer property prediction. *Chemistry of Materials*, 37(18):7002–7013, 2025. 8
- [65] Zhen Zhang, Mianzhi Wang, Yan Huang, and Arye Nehorai. Aligning infinite-dimensional covariance matrices in reproducing kernel hilbert spaces for domain adaptation. In *Proceedings of the IEEE Conference on Computer Vision and Pattern Recognition*, pages 3437–3445, 2018. 2, 5
- [66] Zhen Zhang, Mianzhi Wang, and Arye Nehorai. Optimal transport in reproducing kernel hilbert spaces: Theory and applications. *IEEE transactions on pattern analysis and machine intelligence*, 42(7):1741–1754, 2019. 2, 5
- [67] Jiaqi Zhao, Fei Wang, Kun Li, Yanyan Wei, Shengeng Tang, Shu Zhao, and Xiao Sun. Temporal-frequency state space duality: An efficient paradigm for speech emotion recognition. In *ICASSP 2025-2025 IEEE International Conference on Acoustics, Speech and Signal Processing (ICASSP)*, pages 1–5, 2025. 2
- [68] Hanjing Zhou, Mingze Yin, Wei Wu, Mingyang Li, Kun Fu, Jintai Chen, Jian Wu, and Zheng Wang. Protclip: Function-informed protein multi-modal learning. In *Proceedings of the AAAI Conference on Artificial Intelligence*, pages 22937–22945, 2025. 2, 3

Overview

The supplementary materials provide additional details and elaborations on the datasets used, quantitative analysis experiments, and ablation studies presented in the main manuscript. These topics are organized as follows:

Contents

1. Introduction	2
2. Related Work	2
2.1. Enzyme Kinetic Parameter Prediction	2
2.2. Transformer-based Protein Language Models	3

2.3. Multimodal Integration for Enzyme Modeling	3
3. Methodology	3
3.1. Preliminaries	3
3.2. Molecular Recognition Cross-Attention	4
3.3. Geometry-aware Mixture-of-Experts	4
3.4. Enzyme-Substrate Distribution Alignment	5
3.5. Enzyme Reaction Optimization	6
4. Experiments	6
4.1. Experimental Setup	6
4.2. Performance Analysis	7
4.3. Ablation Study	8
5. Conclusion	8
6. Acknowledgments	9
7. Enzyme Kinetic Parameter Dataset	12
7.1. Details Dataset from [5]	12
7.2. Details OOD Dataset from [43]	12
8. Enzyme Commission Distribution	14
8.1. Overview of EC Class Distributions	14
8.2. Effect of Different Model Architectures Across EC Classes	14
8.3. Impact of Model Size within the ESM Architecture	14
8.4. Conclusion	14
9. Error Distribution Analysis	14
9.1. Overview of Error Distributions	14
9.2. Performance of Ankh3-5.7B and Its Unique Behavior on K_m	14
9.3. ESM2-3B: Best Overall Performance with ERBA	15
9.4. Comparison with Smaller ESM2 Variants	15
10 Explainable Analysis	15
11 Additional Ablation Studies	17
11.1 Stage 1: Does MRCA Help Recognition?	17
11.2 Stage 2: Is Geometry-aware MoE Necessary?	17
11.3 Does ESDA Stabilize Fine-tuning?	17
11.4 Overall	17

7. Enzyme Kinetic Parameter Dataset

7.1. Details Dataset from [5]

In the main experiments of our manuscript, we employ three specially curated kinetic endpoint datasets, as shown in Table 5, to construct and evaluate learning-based models for predicting enzyme kinetic parameters. The raw data underlying the three endpoint datasets were curated from two authoritative biochemical databases: BRENDA [42] release

2022_2 and SABIO-RK [54] as of November 2023. This construction aims to provide an expanded and standardized resource for the field of enzyme kinetic parameter prediction, thereby promoting the systematic development and fair benchmarking of enzyme kinetic prediction models.

The datasets focus on three primary enzyme kinetic parameters: the turnover number (k_{cat}), Michaelis constant (K_m), and inhibition constant (K_i), based on in vitro measurements of wild-type enzymes. Specifically, the datasets include:

- 23,151 entries for Kinetic Parameter k_{cat} ;
- 41,174 entries for Kinetic Parameter K_m ;
- 11,929 entries for Kinetic Parameter K_i .

The construction of these datasets introduces several improvements:

① Data Selection and Standardization: When multiple experimental measurements exist for the same enzyme-substrate pair, the highest value is retained for k_{cat} to capture optimal reaction conditions. For K_m and K_i , the geometric mean is used, reflecting better consistency and stability for binding affinity measurements.

② Diversity of Enzyme Sequences: These datasets significantly expand enzyme sequence diversity compared to previous datasets. They cover a broader range of enzyme families, particularly at the first Enzyme Commission (EC) level, without overrepresenting any specific categories. This is an important step towards fair and comprehensive benchmarking.

③ Link to Structural Data: Each entry is linked to a predicted three-dimensional structure of the corresponding enzyme. In cases where structures are not available in AlphaFold-2.0 [?], ESMFold [30] is used to generate these models. This ensures that structural context is available for all entries, further enriching the dataset for model training.

④ Supporting Fair Benchmarking: By standardizing and expanding the sequence and structure coverage, the dataset offers a more representative resource for enzyme kinetic parameter prediction. This makes it well-suited for developing and fairly evaluating learning-based models in the field.

Overall, this expanded dataset not only enhances the diversity of enzyme sequences but also ensures consistency and stability in model training by using a representative value for each enzyme-substrate pair. Compared to prior works like DLKcat [28] and TurNup [26], our dataset covers a broader range of enzyme families and provides a more comprehensive foundation for large-scale enzyme kinetic predictions.

7.2. Details OOD Dataset from [43]

To evaluate the out-of-distribution (OOD) generalization performance of our model, we utilize two enzyme kinetic datasets focused on k_{cat} and K_m , compiled from the

Class	Kinetic Dataset			Total	Details
	k_{cat}	K_m	K_i		
<i>Dataset I (Main Test): k_{cat}, K_m and K_i from [5]</i>					
Entries	23,151	41,174	11,929	76,254	
EC 1 Oxidoreductases	7,756	13,931	2,744	24,431	Oxidoreductases catalyze diverse redox reactions by transferring electrons between molecules and substrates, and represent the largest EC class with broad kinetic and functional diversity.
EC 2 Transferases	4,155	10,182	2,706	17,043	Transferases catalyze the transfer of functional groups between diverse substrates, enabling the formation of new chemical bonds and the rapid and efficient interconversion of molecules.
EC 3 Hydrolases	8,065	11,025	4,083	23,173	Hydrolases catalyze the hydrolysis of diverse chemical bonds in biological molecules. They efficiently cleave covalent linkages in various substrates with variable enzyme kinetic parameters.
EC 4 Lyases	1,620	2,962	1,525	6107	Lyases catalyze the cleavage of chemical bonds without hydrolysis or oxidation. They form double bonds or ring structures in substrates.
EC 5 Isomerases	928	1,311	434	2,673	Isomerases catalyze the conversion of molecules into their isomeric forms by reorganizing atomic connectivity within the same substrate.
EC 6 Ligases	590	1,363	254	2,207	Ligases catalyze the formation of covalent bonds between two different molecules using chemical energy from nucleotide triphosphates.
EC 7 Translocases	16	98	23	137	Translocases catalyze the active transport of ions or molecules across biological membranes, efficiently coupled with chemical reaction energy.
Unclassified/Invalid	21	302	160	483	Entries that are unclassified or contain format errors, excluded from standard EC categorization.
Unique Sequences	7,183	12,355	2,829	22,367	
Unique EC Classes	2,657	3,550	1,306	7,513	
Unique Organisms	1,685	2,419	652	4,756	
<i>Dataset II (OOD Test): k_{cat} and K_m from [43]</i>					
Entries	35,147	29,321	-	64,468	-
EC 1 Oxidoreductases	12,197	9,770	-	21,967	Oxidoreductases catalyze diverse redox reactions by transferring electrons between molecules and substrates, and represent the largest EC class with broad kinetic and functional diversity.
EC 2 Transferases	8,148	7,820	-	15,968	Transferases catalyze the transfer of functional groups between diverse substrates, enabling the formation of new chemical bonds and the rapid and efficient interconversion of molecules.
EC 3 Hydrolases	8,372	6,537	-	14,909	Hydrolases catalyze the hydrolysis of diverse chemical bonds in biological molecules. They efficiently cleave covalent linkages in various substrates with variable enzyme kinetic parameters.
EC 4 Lyases	3,264	2,510	-	5,774	Lyases catalyze the cleavage of chemical bonds without hydrolysis or oxidation. They form double bonds or ring structures in substrates.
EC 5 Isomerases	1,854	1,367	-	3,221	Isomerases catalyze the conversion of molecules into their isomeric forms by reorganizing atomic connectivity within the same substrate.
EC 6 Ligases	1,252	1,187	-	2,439	Ligases catalyze the formation of covalent bonds between two different molecules using chemical energy from nucleotide triphosphates.
EC 7 Translocases	60	130	-	190	Translocases catalyze the active transport of ions or molecules across biological membranes, efficiently coupled with chemical reaction energy.

Table 5. Detailed breakdown of the enzyme kinetic datasets from [5, 43] used for training and out-of-distribution (OOD) testing. We provide the number of entries, unique sequences, EC classes, organisms, and additional information for each enzyme class in the main and OOD test datasets.

BRENDA and SABIO-RK databases as collected by [43] in Table 5. Each data entry contains enzyme sequences, substrate information, and experimentally measured kinetic parameters.

1 Data Curation and Filtering: The initial collections contained 143,473 entries for k_{cat} and 75,149 entries for K_m . To ensure biological relevance, every protein sequence was mapped to a unique UniProt ID, and sequences lacking a valid or unambiguous ID were excluded. Substrate names

were cross-referenced with KEGG [?] and PubChem [?] to obtain standardized 2D molecular structures. These substrates were then converted into canonical SMILES using RDKit [?]. Any substrates with ambiguous or unresolvable identities were discarded to maintain chemical consistency.

2 Inclusion of Mutant Enzymes: Mutant enzyme variants were retained in the dataset. While K_m showed minimal differences between wild-type and mutant enzymes, k_{cat} distributions revealed that mutant enzymes typically ex-

hibit significantly reduced catalytic activity and efficiency compared to wild-type counterparts.

⑤ **Final dataset composition:** After rigorous screening, the final dataset comprised 35,147 k_{cat} records and 29,321 K_{m} records, with one-tenth allocated as a test set for evaluation.

④ **3D Structure Generation for OOD Testing:** Notably, we use the k_{cat} and K_{m} test sets from [43] for out-of-distribution generalization testing. The corresponding 3D structures for the enzymes are generated using OpenFold [1] or ESMFold [30], ensuring that the structural data is consistent with the latest advancements in protein structure prediction.

8. Enzyme Commission Distribution

This section explores the performance of various models across different Enzyme Commission (EC) classes, focusing on the influence of model architecture and the impact of our **ERBA (Enzyme-Reaction Bridging Adapter)** in improving predictions for enzyme kinetic parameters.

8.1. Overview of EC Class Distributions

Enzyme Commission (EC) classes group enzymes based on their catalytic functions, and understanding the distribution of these enzymes across various EC classes is crucial for predicting their kinetic parameters accurately. The datasets used in this experiment cover a wide range of EC classes, from EC 1 (Oxidoreductases) to EC 6 (Ligases), and include kinetic data for k_{cat} , K_{m} , and K_{i} . Each class includes different numbers of entries, with EC 3 (Hydrolases) containing the most data, and EC 6 (Ligases) containing fewer. The purpose of this analysis is to evaluate how different model backbones and ERBA impact the prediction performance across these classes. It is notable that EC 7 (Translocases) is excluded from the analysis due to insufficient data.

8.2. Effect of Different Model Architectures Across EC Classes

Table 6 presents a comparison of various models across six EC classes, with a focus on the performance metrics R^2 , PCC, RMSE, and MAE for k_{cat} , K_{m} , and K_{i} . We observe that larger backbone models, such as Ankh3-5.7B [2] and ProtT5-3B [18], outperform smaller models, like ESM2-650M, across all EC classes, suggesting that larger models are better equipped to handle the complexities of enzyme-substrate interactions. In EC 1 (Oxidoreductases), Ankh3-5.7B achieves a higher R^2 score for k_{cat} (0.52) compared to ESM2-650M ($R^2 = 0.45$). This indicates that larger backbone models are better at capturing the intricate relationships between enzyme sequences and substrate properties.

8.3. Impact of Model Size within the ESM Architecture

Focusing specifically on the ESM2 architecture, we examine how different model sizes affect performance. As shown in (c) and (d), increasing the model size from ESM2-650M to ESM2-3B leads to noticeable improvements in performance across EC classes. For instance, in EC 5 (Isomerases), the R^2 score for k_{cat} improves from 0.48 with ESM2-650M to 0.50 with ESM2-3B. This performance increase reflects the enhanced capacity of larger models to process more complex enzyme-substrate interactions, which are particularly important in enzyme families with diverse substrates like EC 5 and EC 6.

8.4. Conclusion

The results demonstrate that larger backbone models, such as Ankh3-5.7B and ProtT5-3B, perform better across diverse EC classes, highlighting the importance of model size in capturing complex enzymatic processes. In the case of ESM2, increasing the model size from ESM2-650M to ESM2-3B significantly enhances performance, especially in EC classes with diverse substrates, such as EC 5 (Isomerases). Furthermore, the introduction of ERBA provides a substantial boost to model performance by incorporating both substrate recognition and structural adaptation. This underscores the effectiveness of staged conditioning in improving enzyme kinetic predictions and enhancing the model’s generalization capabilities.

9. Error Distribution Analysis

9.1. Overview of Error Distributions

The error distributions across different models (Ankh3-5.7B, ProtT5-3B, ESM2-650M, and ESM2-3B) and their corresponding performance with ERBA are analyzed in terms of absolute prediction error. As shown in Figure 6, all models show an overall improvement when enhanced with ERBA, particularly in terms of 1-Radio_{AE} values, which represent the percentage of predictions with an absolute error smaller than 1.

9.2. Performance of Ankh3-5.7B and Its Unique Behavior on K_{m}

Notably, the Ankh3-5.7B model, while showing lower overall performance compared to ESM2-3B (as observed in the manuscript), performs significantly better in terms of K_{m} predictions. Specifically, the Ankh3-5.7B model achieves a high 1-Radio_{AE} value of 78.82% for K_{m} predictions, indicating a higher proportion of predictions with small errors despite having lower overall R^2 and PCC scores. This suggests that Ankh3-5.7B may be better at making precise predictions within a narrower range of K_{m} values, while other

Index	Class Name	Kinetic Endpoint: k_{cat}				Kinetic Endpoint: K_m				Kinetic Endpoint: K_i			
		R ² ↑	PCC↑	RMSE↓	MAE↓	R ² ↑	PCC↑	RMSE↓	MAE↓	R ² ↑	PCC↑	RMSE↓	MAE↓
<i>(a) Ankh3-5.7B [2] w/ ERBA</i>													
EC-1	Oxidoreductases	0.39	0.68	1.25	0.89	0.51	0.78	0.83	0.61	0.53	0.73	1.29	0.96
EC-2	Transferases	0.44	0.65	1.23	0.87	0.55	0.74	0.78	0.58	0.39	0.65	1.27	0.97
EC-3	Hydrolases	0.45	0.70	1.13	0.85	0.53	0.73	0.85	0.60	0.29	0.60	1.72	1.27
EC-4	Lyases	0.52	0.73	1.20	0.91	0.60	0.79	0.73	0.55	0.54	0.74	1.36	0.99
EC-5	Isomerases	0.42	0.62	1.41	0.95	0.60	0.76	0.85	0.67	0.65	0.82	1.15	0.91
EC-6	Ligases	0.50	0.71	1.01	0.79	0.30	0.55	1.12	0.83	0.27	0.51	1.38	1.08
<i>(b) ProtT5-3B [11] w/ ERBA</i>													
EC-1	Oxidoreductases	0.40	0.71	1.44	0.99	0.60	0.79	0.77	0.58	0.55	0.73	1.25	0.98
EC-2	Transferases	0.48	0.73	1.25	0.90	0.51	0.69	0.79	0.58	0.42	0.69	1.39	1.03
EC-3	Hydrolases	0.42	0.69	1.20	0.89	0.50	0.71	0.94	0.69	0.46	0.68	1.41	1.04
EC-4	Lyases	0.48	0.70	1.21	0.85	0.53	0.71	0.87	0.65	0.69	0.83	1.07	0.77
EC-5	Isomerases	0.46	0.70	1.29	0.90	0.63	0.80	0.80	0.61	0.65	0.81	1.10	0.89
EC-6	Ligases	0.54	0.79	0.92	0.67	0.40	0.65	0.97	0.71	0.41	0.65	1.30	0.97
<i>(c) ESM2-650M [30] w/ ERBA</i>													
EC-1	Oxidoreductases	0.35	0.62	1.37	1.05	0.43	0.67	1.01	0.77	0.51	0.72	1.28	0.98
EC-2	Transferases	0.39	0.66	1.34	1.02	0.34	0.62	0.96	0.74	0.35	0.60	1.39	1.05
EC-3	Hydrolases	0.40	0.65	1.32	1.01	0.33	0.60	1.05	0.80	0.31	0.65	1.71	1.29
EC-4	Lyases	0.44	0.69	1.28	0.98	0.31	0.58	1.00	0.77	0.46	0.74	1.47	1.10
EC-5	Isomerases	0.43	0.65	1.32	0.99	0.53	0.77	0.90	0.81	0.71	0.87	1.12	0.88
EC-6	Ligases	0.50	0.71	0.99	0.79	0.33	0.57	1.09	0.85	0.32	0.60	1.41	1.08
<i>(d) Ours (ESM2-3B [30] w/ ERBA)</i>													
EC-1	Oxidoreductases	0.37	0.62	1.32	0.95	0.55	0.74	0.90	0.69	0.58	0.77	1.19	0.92
EC-2	Transferases	0.46	0.69	1.22	0.87	0.53	0.73	0.81	0.61	0.38	0.65	1.37	0.99
EC-3	Hydrolases	0.43	0.68	1.18	0.88	0.51	0.72	0.90	0.65	0.48	0.71	1.50	1.10
EC-4	Lyases	0.50	0.71	1.27	0.92	0.56	0.75	0.81	0.61	0.65	0.81	1.19	0.84
EC-5	Isomerases	0.46	0.73	1.39	0.94	0.61	0.78	0.84	0.64	0.67	0.83	1.20	0.95
EC-6	Ligases	0.53	0.77	0.96	0.71	0.34	0.59	1.02	0.76	0.34	0.62	1.39	1.03

Table 6. Performance Comparison Across Enzyme Commission Classes. The table compares the performance of different backbone models and the impact of ERBA on kinetic parameter prediction for six EC classes: EC 1 (Oxidoreductases), EC 2 (Transferases), EC 3 (Hydrolases), EC 4 (Lyases), EC 5 (Isomerases), and EC 6 (Ligases). Metrics include R², PCC, RMSE, and MAE for k_{cat} , K_m , and K_i , showcasing the effect of model size and architecture on the predictive accuracy across enzyme classes.

models may struggle with broader generalization across the K_m space.

9.3. ESM2-3B: Best Overall Performance with ERBA

The ESM2-3B model consistently outperforms all other backbones, particularly for k_{cat} and K_m . The error distributions show that the ESM2-3B with ERBA achieves the highest 1-RadiusAE values (67.67% for k_{cat} , 79.53% for K_m , and 62.28% for K_i), demonstrating its robust performance across all three kinetic endpoints. This confirms the effectiveness of the ESM2-3B backbone combined with ERBA for enzyme kinetic parameter prediction.

9.4. Comparison with Smaller ESM2 Variants

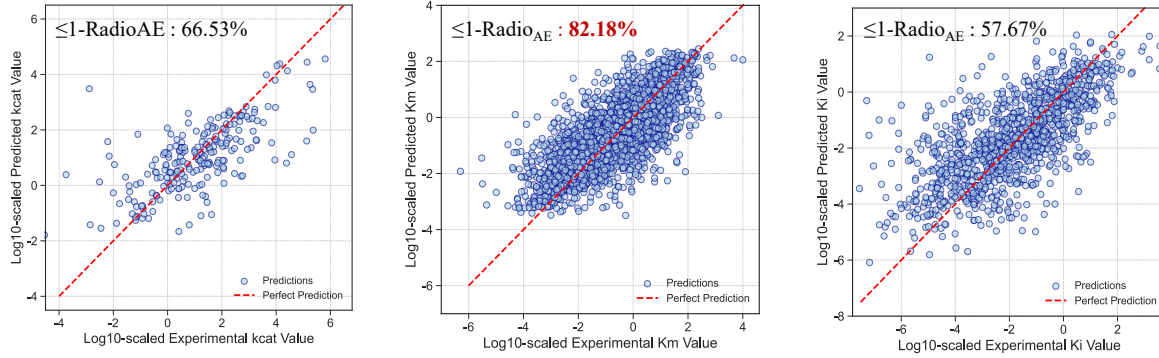
Interestingly, while the larger models like ESM2-3B excel overall, the smaller versions (such as ESM2-650M) show a reduction in the percentage of predictions with smaller errors, especially for K_m . This highlights the trade-off between model size and accuracy for out-of-distribution gen-

eralization. Larger models tend to perform better overall but may exhibit more variability in specific kinetic parameter predictions, particularly in smaller enzyme classes or in scenarios with less data.

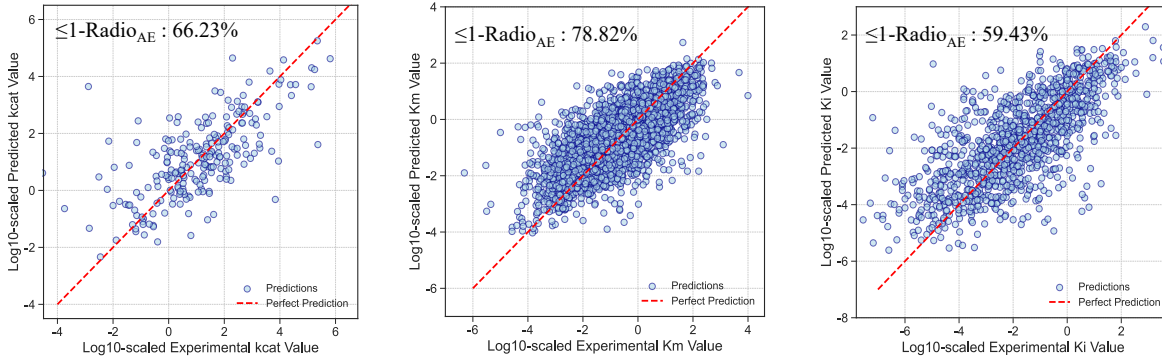
10. Explainable Analysis

We further analyze the interpretability of our method through the visualization of module behaviors. We further analyze the interpretability of our method through the visualization of module behaviors. In Figure 7, MRCA produces highly localized attention regions on the sequence and assigns the highest scores to chemically functional groups on the substrate. In Figure 8, the gating distribution is sparse and dynamically relies on enzyme characteristics, while 3D saliency map shows that top-1 expert responses cluster around the adaptive binding pocket.

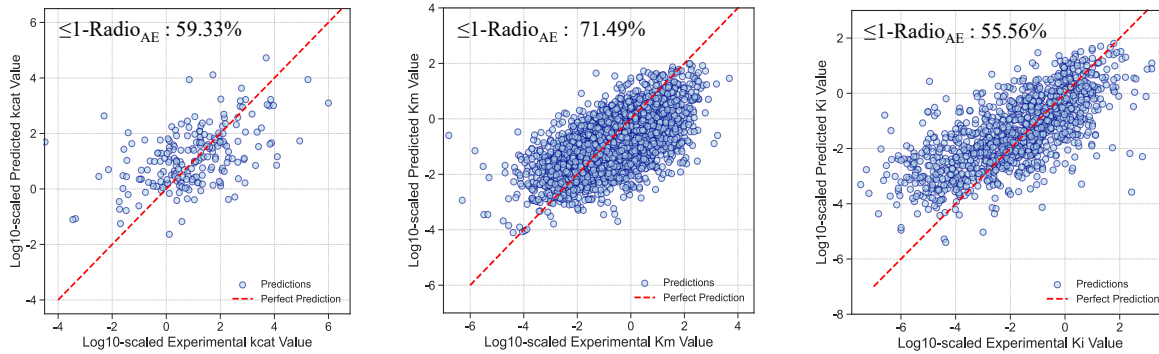
(a) Error Distribution of *Ankh3-5.7B* w/ERBA



(b) Error Distribution of *ProtT5-3B* w/ERBA



(c) Error Distribution of *ESM2-650M* w/ERBA



(d) Ours (Error Distribution of *ESM2-3B* w/ERBA)

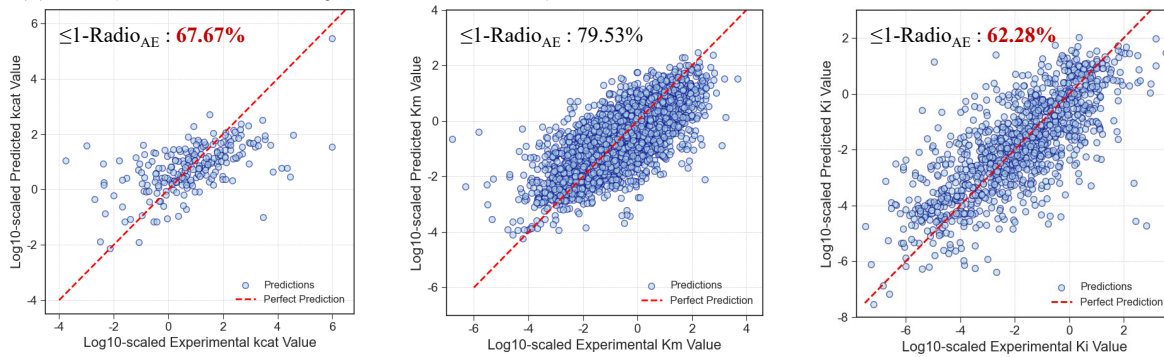


Figure 6. Error Distribution Comparison Across Different Backbone Models and ESM Sizes. It shows the error distribution of predicted versus experimental values for three kinetic parameters (k_{cat} , K_m , and K_i) across four backbone models: (a) *Ankh3-5.7B* [2], (b) *ProtT5-3B* [11], (c) *ESM2-650M* [30], and (d) *ESM2-3B* [30], each augmented with ERBA. The plots show the proportion of predictions with absolute error less than or equal to 1, denoted as 1-Radio_{AE} .

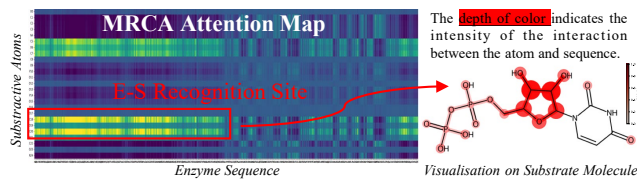


Figure 7. Visualization of MRCA.

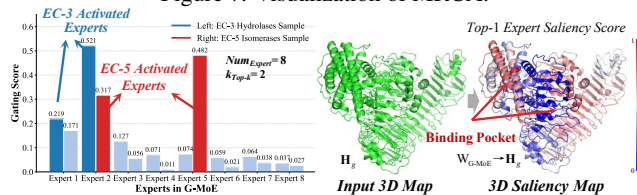


Figure 8. Visualization of G-MoE.

Stage 1	Method	Kinetic Endpoint: K_i			
		$R^2 \uparrow$	PCC \uparrow	RMSE \downarrow	MAE \downarrow
	w/ Concat & Self-Attention [?]	0.47	0.69	1.44	1.10
	w/ MRCA (Ours)	0.61	0.78	1.26	0.91

Table 7. Stage 1 (Recognition) ablation on K_i : Replacing *Concat* & *Self-Attention* with our MRCA markedly improves R^2 and PCC while reducing RMSE/MAE under identical settings.

Stage 2	Method	Kinetic Endpoint: K_i			
		$R^2 \uparrow$	PCC \uparrow	RMSE \downarrow	MAE \downarrow
	w/ MoE [?]	0.50	0.71	1.39	1.05
	w/ G-MoE (Ours)	0.61	0.78	1.26	0.91

Table 8. Stage 2 (Adaptation) ablation on K_i : *standard MoE* vs. our G-MoE that routes by pocket geometry; geometry-aware experts yield consistent gains across all metrics.

Optimization	Method	Kinetic Endpoint: K_i			
		$R^2 \uparrow$	PCC \uparrow	RMSE \downarrow	MAE \downarrow
	w/ \mathcal{L}_2 Loss [?]	0.48	0.69	1.42	1.08
	w/ ESDA (Ours)	0.61	0.78	1.26	0.91

Table 9. Objective ablation on K_i : *plain \mathcal{L}_2* vs. ESDA-regularized objective. Distribution alignment in RKHS stabilizes fine-tuning and improves R^2 /PCC while lowering RMSE/MAE.

11. Additional Ablation Studies

To isolate the contribution of each component, we ablate on K_i prediction under identical preprocessing, backbone, and training schedule. Across all studies, each module provides measurable gains and the full model is consistently best.

11.1. Stage 1: Does MRCA Help Recognition?

We replace the common *Concat & Self-Attention* [?] fusion with our MRCA, as shown in Table 7, which explicitly conditions enzyme tokens on substrate tokens in the PLM latent space before any structural input. MRCA improves R^2 from 0.47 to **0.61** (+0.14 / $\uparrow 29.8\%$), PCC from 0.69 to **0.78** (+0.09 / $\uparrow 13.0\%$), and reduces RMSE from 1.44 to **1.26** ($\downarrow 12.5\%$) and MAE from 1.10 to **0.91** ($\downarrow 17.3\%$). Results indicate that conditioning the PLM on substrate identity early yields a cleaner recognition signal than shallow concatena-

tion, which underuses PLM priors.

11.2. Stage 2: Is Geometry-aware MoE Necessary?

As shown in Table 8, we compare a *standard MoE* [?] against our G-MoE, which routes by pocket geometry and applies pocket-local, low-rank adaptation. G-MoE raises R^2 0.50 \rightarrow **0.61** (+0.11 / $\uparrow 22.0\%$) and PCC 0.71 \rightarrow **0.78** (+0.07 / $\uparrow 9.9\%$), while lowering RMSE 1.39 \rightarrow **1.26** ($\downarrow 9.4\%$) and MAE 1.05 \rightarrow **0.91** ($\downarrow 13.3\%$). This validates that the geometry-routed experts specialize to distinct conformational regimes (pocket size/shape/flexibility), outperforming a single shared adaptation rule.

11.3. Does ESDA Stabilize Fine-tuning?

We replace the plain \mathcal{L}_2 regression with our ESDA objective, reported in Table 9, which aligns the distributions of $\mathbf{H}^{(0)}$ (sequence), $\mathbf{H}^{(1)}$ (seq+substrate), and $\mathbf{H}^{(2)}$ (seq+substrate+structure) to the PLM manifold via RKHS MMD. ESDA improves R^2 0.48 \rightarrow **0.61** (+0.13 / $\uparrow 27.1\%$) and PCC 0.69 \rightarrow **0.78** (+0.09 / $\uparrow 13.0\%$), and reduces RMSE 1.42 \rightarrow **1.26** ($\downarrow 11.3\%$) and MAE 1.08 \rightarrow **0.91** ($\downarrow 15.7\%$). Thus, the distribution alignment curbs feature flooding from strong structural cues and preserves pretrained biochemical semantics during adaptation.

11.4. Overall

Gains accumulate across stages: MRCA supplies substrate-aware recognition, G-MoE injects pocket-specific adaptation, and ESDA keeps both anchored to the PLM’s semantic space, yielding the best accuracy and lowest errors on K_i .